3 Excess facular emission from an isolated active region: AR 7978[1]

We study the facular contribution to solar irradiance variations on the short time scale by analyzing a simple case of the isolated active region NOAA AR 7978 that crossed the solar disk during the 1996 minimum of activity. Its passage during seven Carrington Rotations (CR), from its birth during CR 1911 to its full dispersion during CR 1917, allows us to analyze the evolution of the angular distribution of the excess radiance of the facular region using SOHO/VIRGO and MDI data. We associate this evolution with the changes on the spatial extent of this active region as well as with its aging. Finally, we evaluate the total (that means in all directions) emission of this facular region and its spectral and temporal evolution.

3.1 Introduction

A large fraction of the solar irradiance variations are induced by the presence and evolution of the sunspots and faculae present over the solar disk and, probably, by the photospheric network and small features of the magnetic field (see, e.g., Foukal & Lean 1988; Solanki 1994; Fröhlich & Lean 1998a). The supporting evidence has been obtained by statistical treatment of observations and the utilization of proxy data, such as plage and longitudinal magnetic field along the line of sight in the photosphere. Progress in the understanding of the variation of the solar energy output needs studying the radiative components associated with photospheric magnetic field features in active regions and outside them (Topka et al. 1992, 1997).

[1]This Chapter is based on: Ortiz, A., Domingo, V., Sanahuja, B. & Fröhlich, C., submitted to Journal of Atmospheric and Solar-Terrestrial Physics.

Steinegger et al. (1996), for example, have studied the energy balance of the emission by active regions from a combination of direct measurements from space and ground observatories proxies.

During the second half of 1996, coinciding with the solar minimum between cycles 22 and 23, ongoing solar activity was essentially governed by a single AR, identified as NOAA AR 7978. This region appeared in July 1996, and until November 1996, only a few small, short-lived AR's were observed on the solar disk, apart from AR 7978; thus, solar activity during this period came mainly from this active region. This fact converts AR 7978 in a perfect target AR, providing a unique opportunity to study the evolution of the excess radiance produced by an evolving active region. Because of its privileged characteristics, this AR has been studied in detail with different purposes by Harvey & Hudson (2000), Démoulin et al. (2002) and van Driel-Gesztelyi et al. (2003). We present a first example of continued monitorization of the irradiance variations produced from a single active region. We analyze the relationship between the evolution of the radiance of the active region, the evolution of the photospheric magnetic field and the total solar irradiance variations using data from the VIRGO and MDI instruments on board the SOHO satellite.

The VIRGO instrument (Fröhlich et al. 1995) measures the total solar irradiance as well as the spectral solar irradiance at three wavelength bands. VIRGO incorporates the Low-resolution Oscillations Imager (LOI), a telescope that produces an image of the sun at 500 nm, over a 16-pixel detector, four of which are used for image stabilization. In addition, the SOI-MDI instrument (Scherrer et al. 1995) obtains solar magnetograms and irradiance measurements, at 676.8 nm (continuum around the Ni I spectral line), with two arc-seconds pixel resolution (see Chapter 2).

3.2 Data sets and observations

MDI magnetograms have been used to determine the characteristics of the magnetic active region. The MDI spectral intensity images have been used to determine the presence of sunspots.

The study of the total and spectral irradiance has been made with the VIRGO data. The angular and spectral distributions have been obtained from the radiometers, SPM and LOI data, and the longitudinal extent of the active region emissions

has been obtained from the LOI data.

The following MDI and VIRGO data sets have been used:

- Full-disk line-of-sight longitudinal magnetograms (1024×1024 pixels); 15 images per day. Provided by MDI.
- Full-disk photospheric intensity continuum images (1024×1024 pixels), at 676.8 nm; 4 images per day. Provided by MDI.
- Total solar irradiance (TSI) measured by the DIARAD and PMO6-V radiometers; hourly averages. Provided by VIRGO.
- Spectral irradiance measured by the sunphotometers (SPMs), at 402, 500, and 862 nm; once per minute (SPM 1.0 data sets). Provided by VIRGO.
- Spectral radiance at 500 nm in the 12 scientific pixels of LOI; once per minute (LOI 0.7c data sets). The measurements of the pixels are limited to about 70° in heliocentric angle because the outer ring of the LOI solar image is cut by the four guiding pixels. Provided by VIRGO.

During Carrington Rotation 1908, a complex of AR's appeared around Carrington longitude (C_L) 250° and lasted for several solar rotations (Harvey & Hudson 2000). On 4 July 1996 a new strong center of magnetic activity emerged within the activity complex, and developed into a region designated as NOAA AR 7978 (CR 1911, S10, C_L=248). This AR finally dispersed during December 1996 (CR 1917), thus being visible for seven rotations. We will keep the region named as AR 7978 along all rotations from 1911 to 1917, although it was denoted as NOAA AR 7981 and NOAA AR 7986 in its second and third disk passages, respectively. After the fourth rotation, this region did not get a NOAA number because it did not show any spots. Therefore, during a large part of its life there were no significant sunspots; in fact, rotations 1913, 1914 and 1915 are particularly sunspot free. These rotations have been used to determine the contribution of the faculae of the region and its evolution with age. Although the AR fully dispersed in CR 1917, we have extended our study only up to CR 1916 because during CR 1917 new magnetic concentrations emerged, that could distort the VIRGO irradiance measurements.

Figures 3.1 and 3.2 show this active region, which lies between Carrington longitudes 250° and 270°. Figure 3.1 presents an ensemble of MDI/SOHO magnetograms,

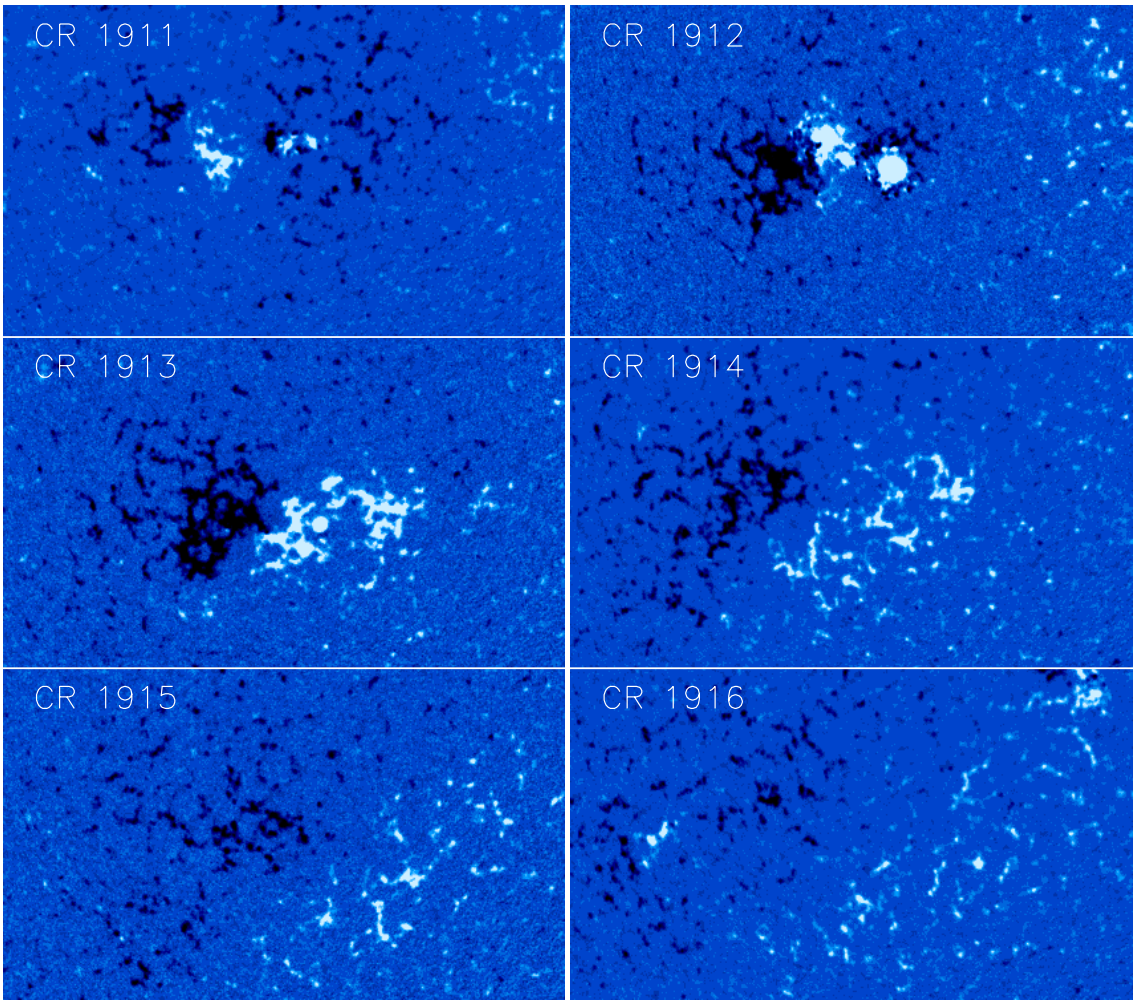

Figure 3.1: Solar magnetograms (line-of-sight magnetic field intensity) obtained by the MDI instrument showing the evolution of the studied AR, NOAA 7978, which emerged on CR 1911 (July 1996) and lasted until CR 1917 (December 1996).

from CR 1911 (July 1996) to CR 1916 (November 1996), each centered on the active region, and illustrates the long-term evolution of the magnetic field of AR 7978 at successive Central Meridian passages (CMP's). The smooth aging of the region from one Carrington rotation to the next is clearly seen, as well as that its extent grows with time. During CR 1912 and CR 1913 two different centers of activity coexist, and there is a transition from a previous active region to a new one during CR 1911. Figure 3.2 represents a sequence of MDI continuum intensity snapshots which show the AR evolution through CR's 1912 and 1913. This region contains sunspots and faculae, the latter being only visible at the limbs; only one small sunspot is still visible in CR 1913 and has vanished in CR's 1914 and 1915.

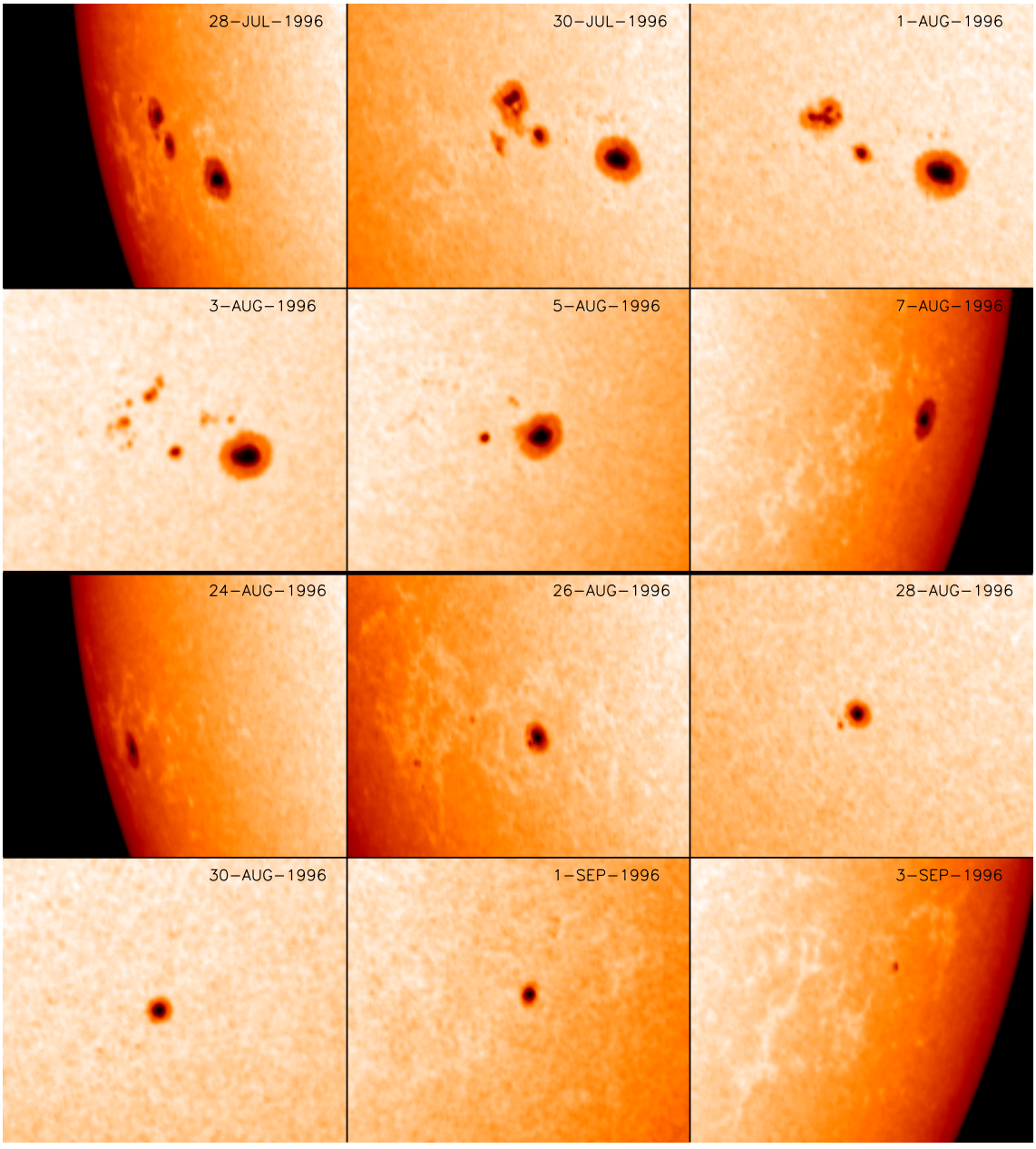

Figure 3.2: Continuum intensity sequence of snapshots measured by MDI, which shows the evolution of the AR through Carrington rotations 1912 and 1913. Note that the sunspot group finally disappears during CR 1913, giving place to Carrington rotations dominated by faculae.

Histograms in figure 3.3 show the evolution with Carrington rotations of the magnetic field distribution. From figures 3.1 and 3.3 we can conclude that: the AR has a smaller extent when it is younger (figure 3.1) while having the highest magnetic field values (CR 1911, 1912 and 1913 in figure 3.3); these CR's are dominated by sunspots (very small in CR 1913). As the active region ages, magnetic field values become lower, faculae start dominating and the AR grows in extent.

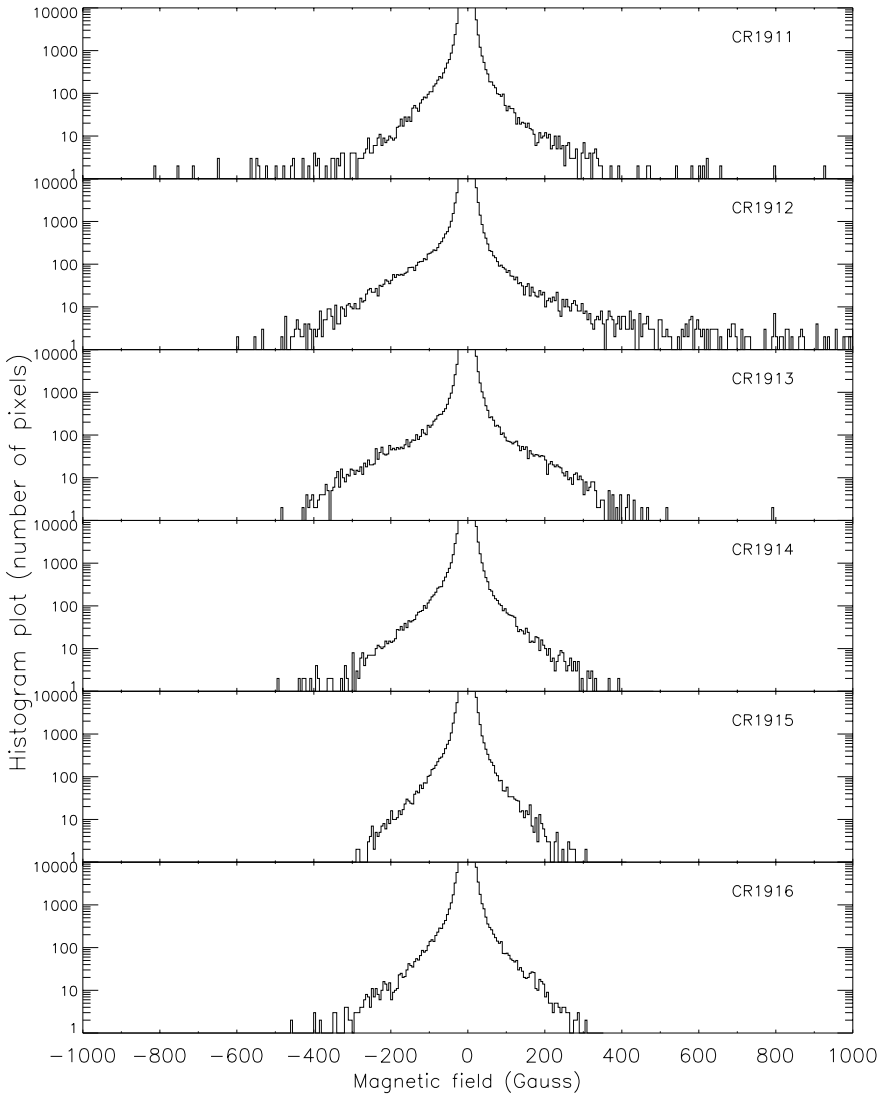

Figure 3.3: Temporal evolution of the distribution of the magnetic field from magnetograms obtained when the AR was near the Central Meridian. For clarity, the number of pixels has been cut at 10^4. Time spans from June to November 1996.

3.3 Evolution of the Angular Distribution

We have focused our analysis in the facular region and its associated excess of irradiance, consequently the presence of a sunspot is interpreted as a distortion in the observations. Figure 3.4 shows the temporal evolution of the angular distribution of the excess spectral radiance at 500 nm as measured by LOI, normalized at 1 AU. In each plot we indicate the day that the center of the AR crossed the central meridian and the latitude of the AR center at CMP. Figures 3.5 to 3.7 represent SPM spectral measurements of the temporal evolution of the center-to-limb flux variations induced by the AR; figure 3.8 shows the bolometric center-to-limb distributions, as measured by the DIARAD and PMO6-V radiometers.

We assume that the AR is the unique source of disturbances of the solar irradiance. The displayed angular distributions have been calculated by representing the excess or deficit of flux or radiance, relative to the quiet Sun, versus the heliocentric angle of the center of the facular region, as it rotates from East to West. Therefore, a null value means that there is no variation related to the background level. Proceeding in this way, we are converting temporal measurements into angular distributions of the observed fluxes or intensities. Two assumptions are made: a) that the intensity of the facular emission is constant during the 13 days it is visible on the disk; b) that the facular region has no extent. We can check how valid is the first assumption as it passes across the disk, by comparing its value when the active region is East or West of the Central Meridian.

A small sunspot observed in MDI photospheric intensity continuum images during CR 1913, becomes almost imperceptible in the angular distribution plots; rotations 1913, 1914 and 1915 apparently show only an excess of radiance. The aging of the active region is clear when we take into account the evolution of the excess radiance of the facular region along these rotations: the older the region, the wider becomes its angular distribution. The limb brightening peaks near 60° for CR 1913 and goes down to 45° for CR 1915. From these plots is also evident that the variations of the spectral irradiance are greater at shorter wavelengths (note the different scales used in figures 3.5 to 3.7). We should keep in mind that a small contribution of the sunspot present in CR 1913 could contaminate the results.

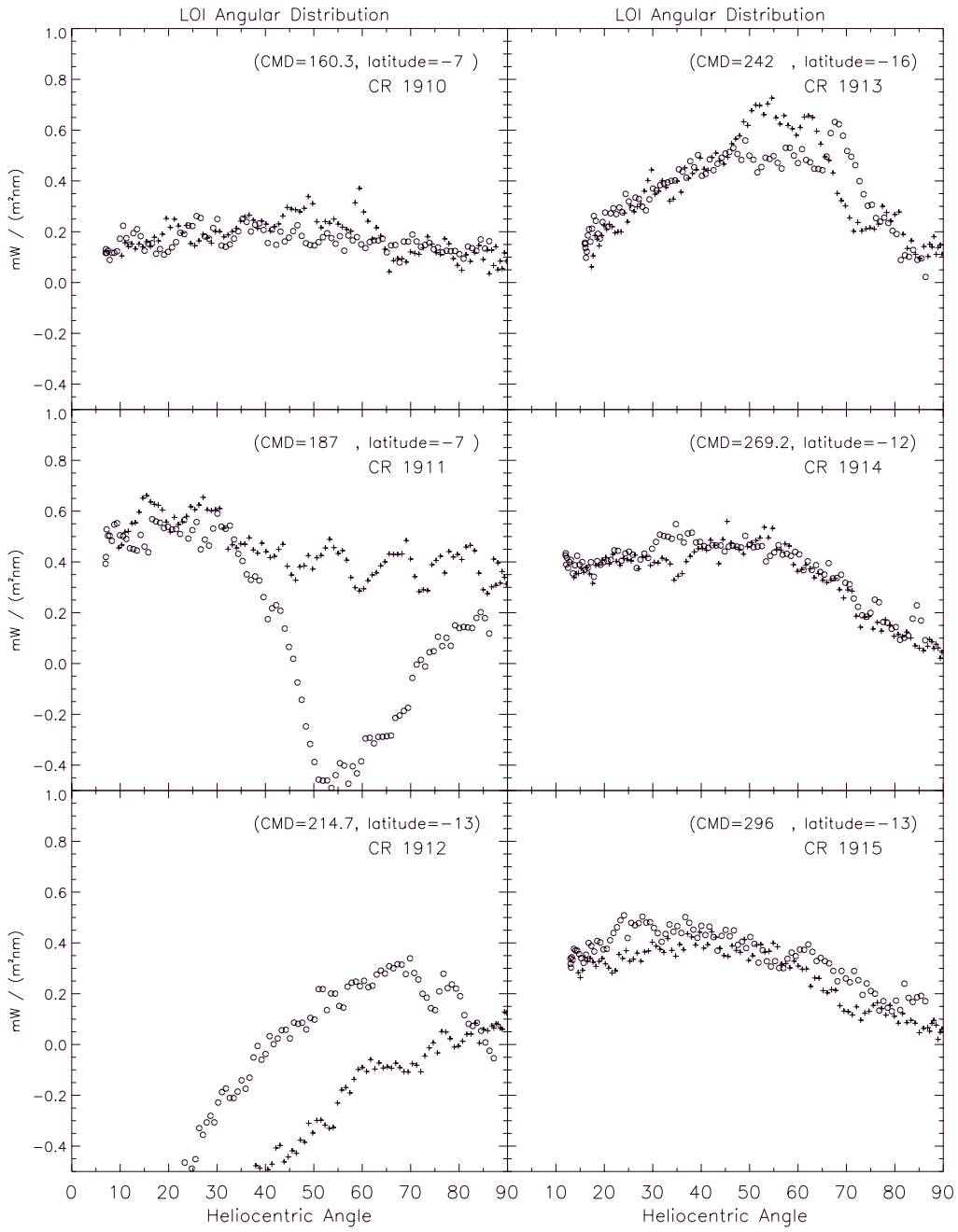

Figure 3.4: LOI measurements of the angular distribution of the excess radiance emitted by AR 7978 from CR 1910 to CR 1915. The abscissa represents the heliocentric angle of the AR center at the moment of the measurement. The different points are obtained as the AR crossed the solar disk from East to West. Points obtained eastward of the central meridian are represented by crosses (+), and points obtained westward of the central meridian by empty circles (∘). The CMD (Central Meridian Day) and latitude of the AR center at the CMP are indicated, as well as the corresponding CR number.

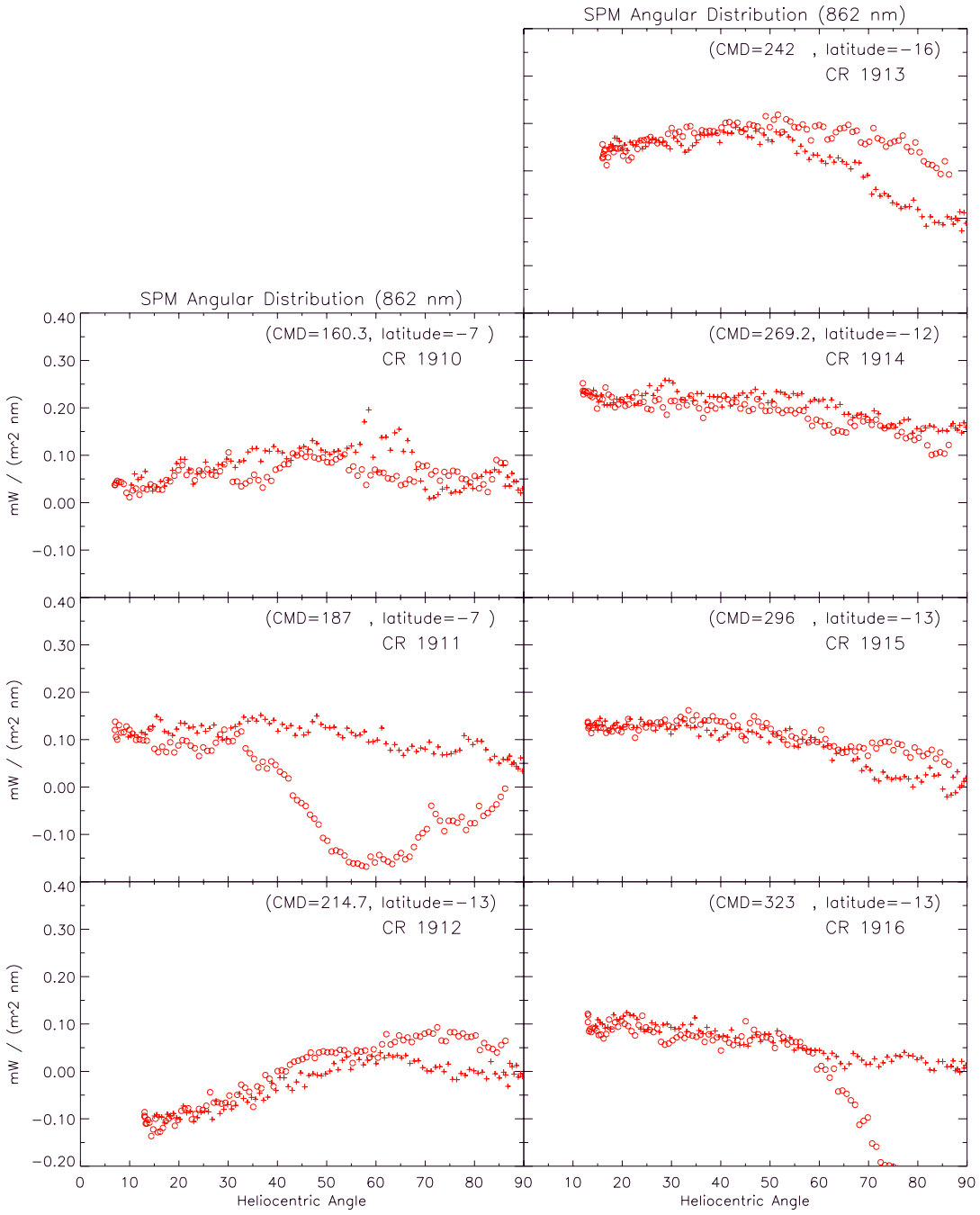

Figure 3.5: Angular distribution of the irradiance variations produced by the AR at 862 nm, as measured by SPM sunphotometers. Symbols represent the same as in figure 3.4.

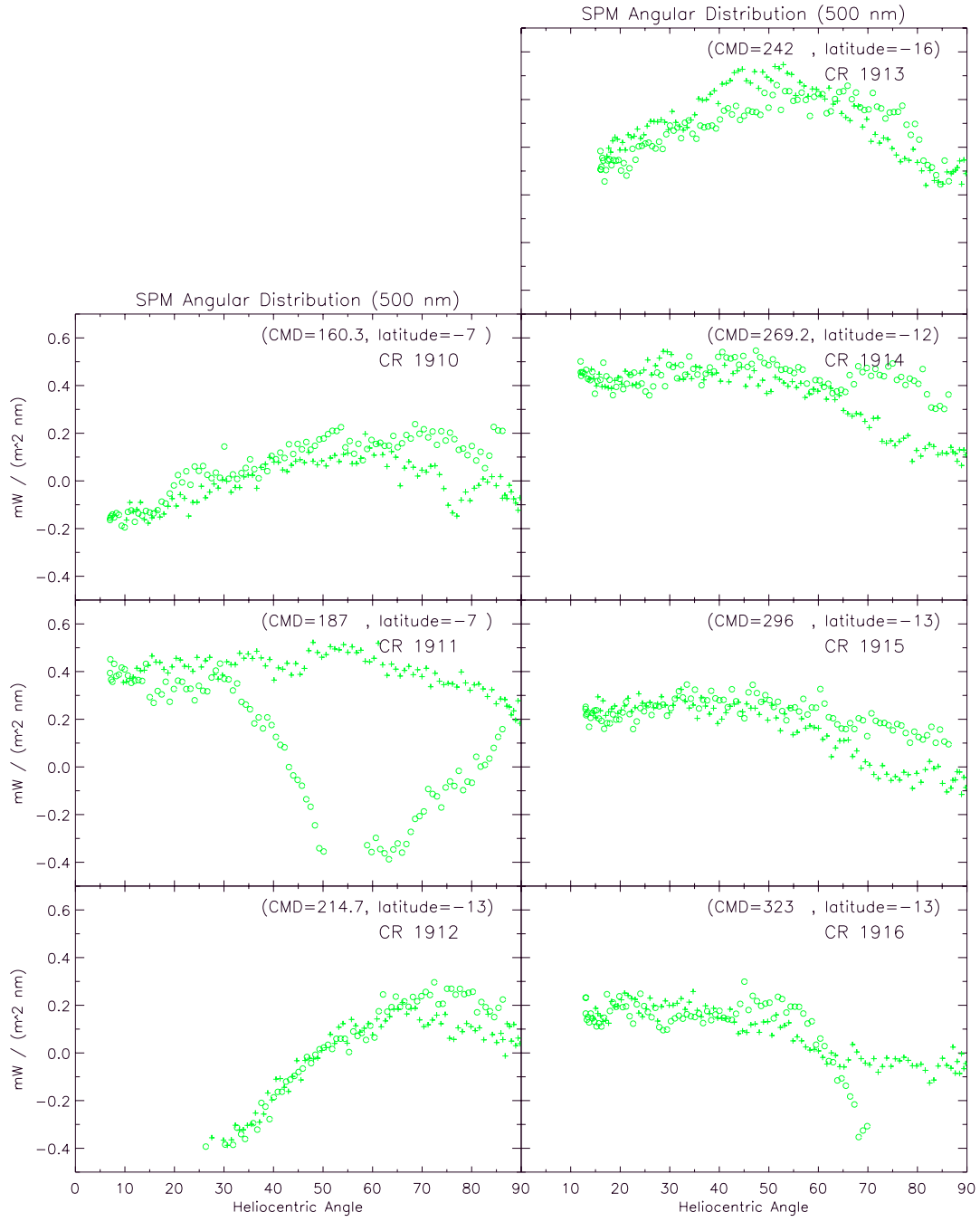

Figure 3.6: Same as figure 3.5 for the 500 nm filter.

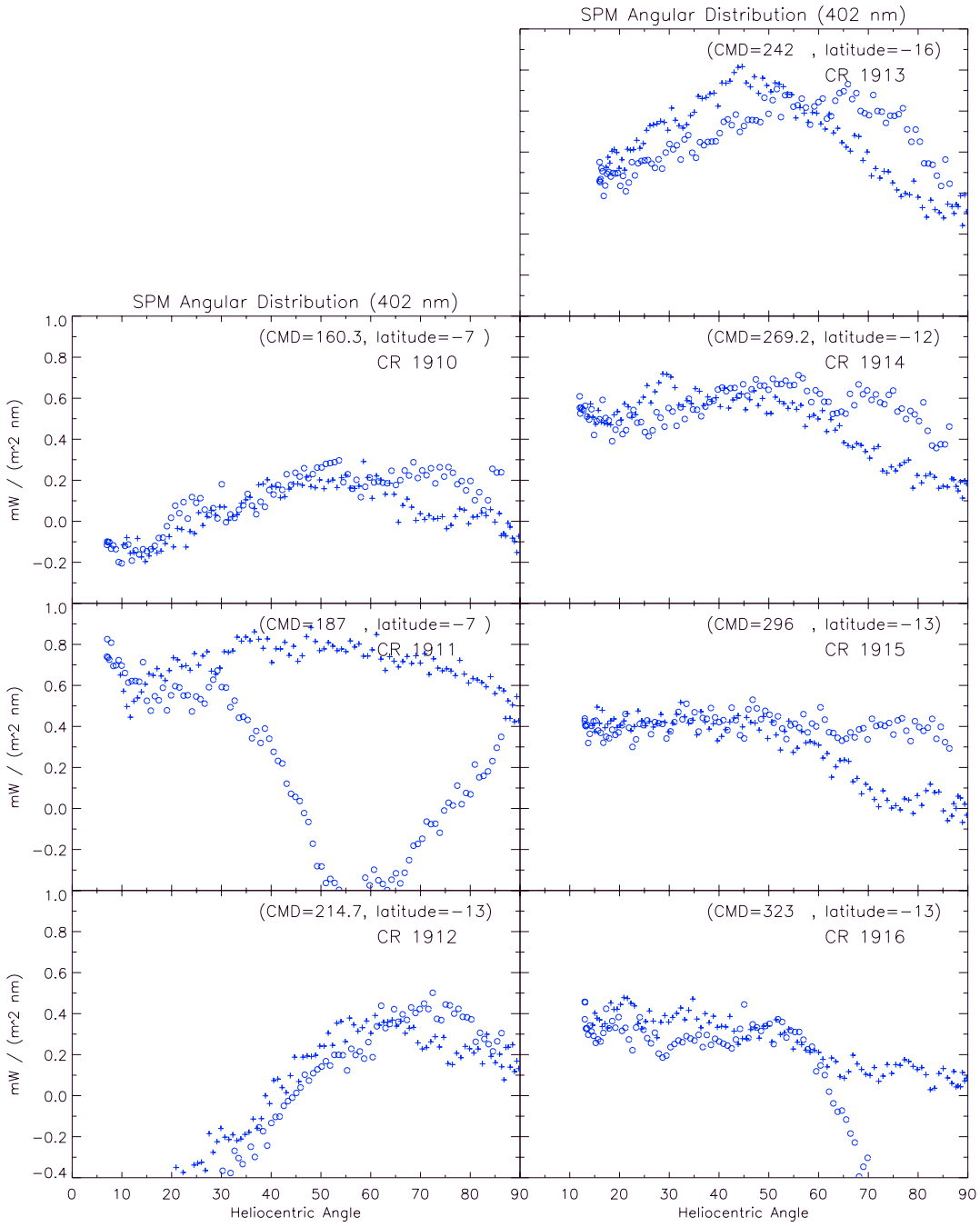

Figure 3.7: Same as figure 3.5 for the 402 nm filter. Note that the greater variations are detected at this wavelength.

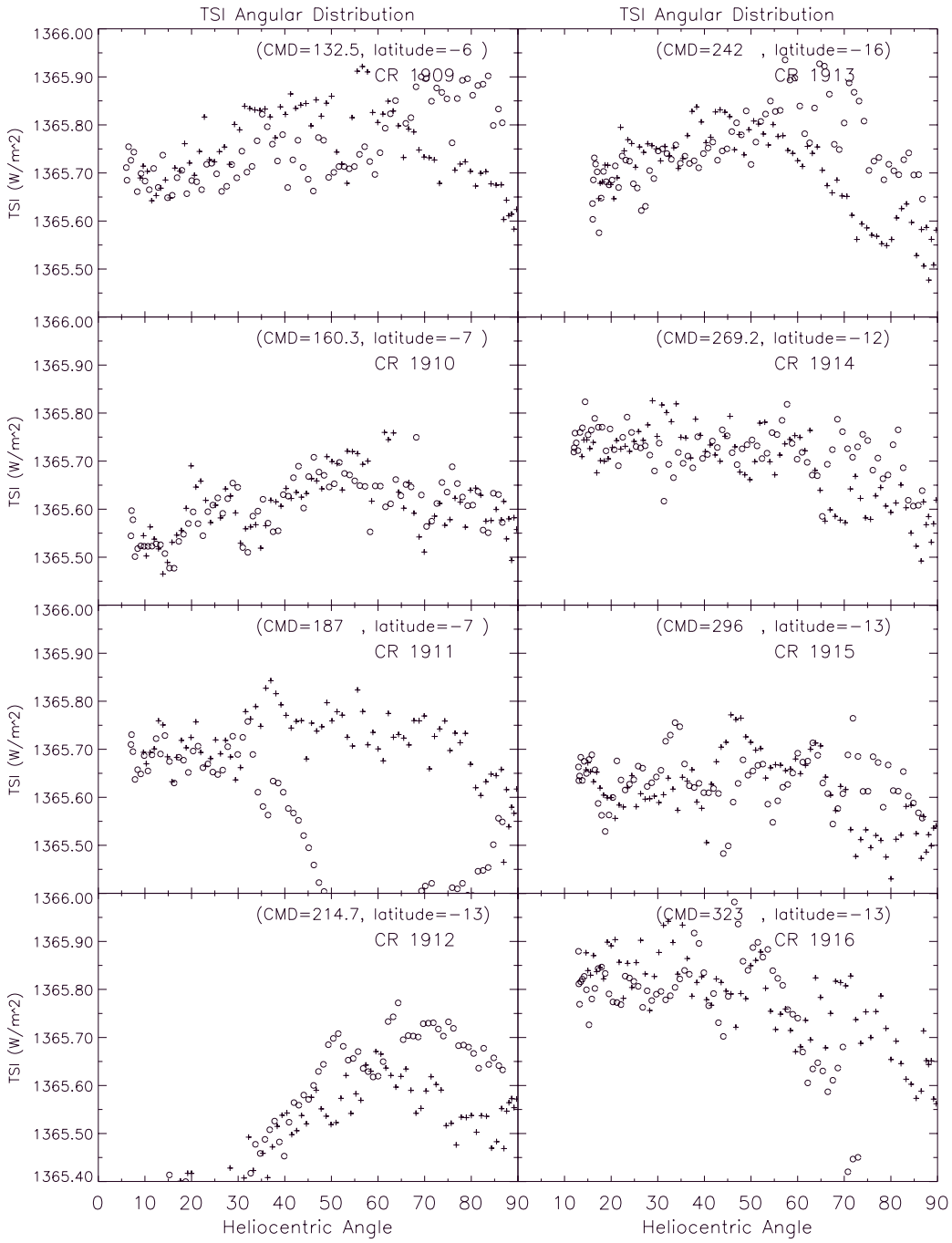

Figure 3.8: Total solar irradiance measurements of the angular distribution of the variations induced by the passage of AR 7978, from CR 1909 (previous to the AR emergence) to CR 1916. Symbols represent the same as in figures 3.4 to 3.7. The passage of sunspots and facular regions is evident.

3.4 Total Facular Emission

We have tried to reproduce the center to limb variation (CLV) of the facular contribution to solar irradiance variations, by fitting phenomenological models to the observed angular distributions. Chapman et al. (1992) compile some of the existing phenomenological models in their work; following this investigation, we have fitted to our observations a function of the form:

$$I(\mu) = \mu(a + b\,\mu + c\,\mu^2) \tag{3.1}$$

where $\mu = \cos\theta$, θ is the heliocentric angle and a, b and c are the limb brightening parameters. Rotating these curves, and assuming that the region emits the radiation in cylindrical symmetry around the vertical to the surface, we obtain a display of the excess facular emission in all directions. Figure 3.9 is a 3-dimensional rendering corresponding to the rotation of two of the fitted curves, i.e. those from CR's 1913 and 1915. The different angular values are obtained as the active region crosses the solar disk; as can be seen, the angular distribution becomes less limb-brightened as the region becomes older and larger.

Solar irradiance variations are induced, at least on time scales of a few solar rotations, by active regions which in turn are strong concentrations of magnetic flux in the solar photosphere. In figure 3.1 we see how the active region spreads out from CR 1913 through 1916. In CR 1912 it coexists with a former active region that had stronger magnetic field intensity. To evaluate the effect of aging on the AR, we have developed the concept of active region extent, which is quantified by means of two parameters: first is the number of pixels within the AR with magnetic field intensity > 80 G (NB); second parameter is the AR surface, in millionths of solar hemisphere, defined as the surface that includes 90% of the pixels with magnetogram signal higher than 80 G (SAR). Figure 3.10 shows the evolution of both parameters (NB, top panel; SAR, bottom panel) along six Carrington rotations; these parameters reflect the evolution of this AR. From this figure we conclude that the total magnetic flux of the region decays as its extent grows with time.

A facular region is composed of many small elements, which are probably individual faculae. Topka et al. (1992, 1997) pursued a detailed study of the small elements with high-resolution images. To compare our measurements with these ob-

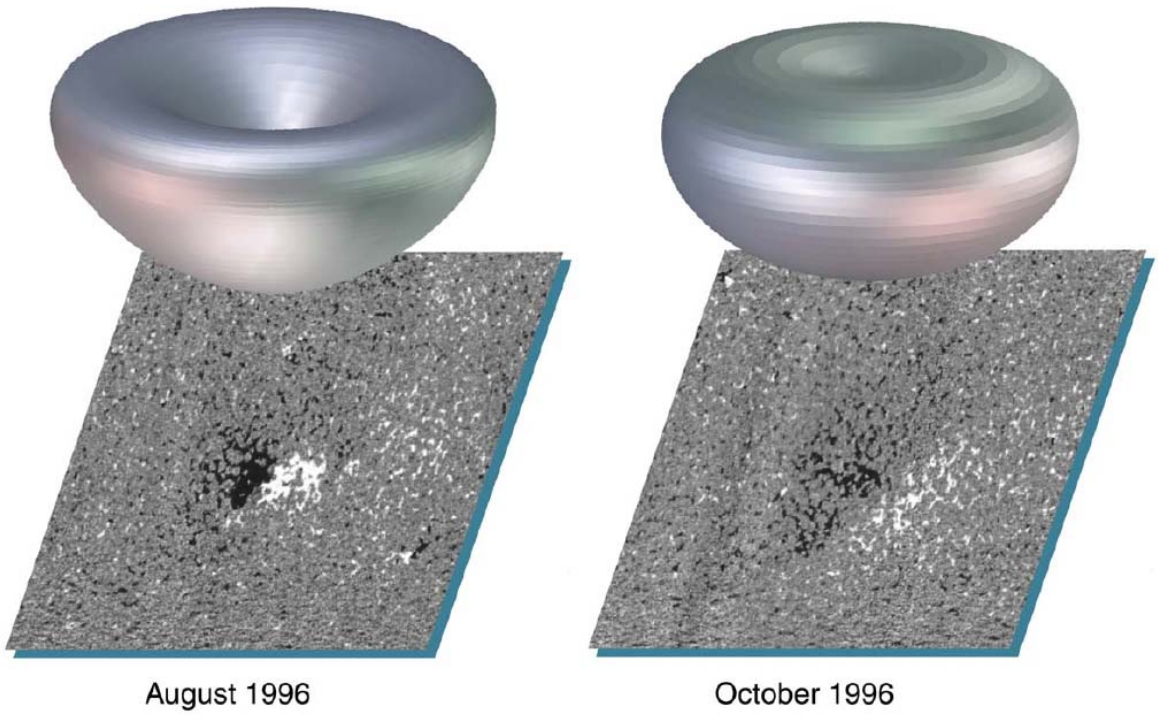

Figure 3.9: Three-dimensional rendering of the angular distribution of the excess irradiance emitted at 500 nm by the studied active region at two stages of its development. The brightening of the facular region is more uniform at the latter stage. The surfaces under the distributions are MDI magnetograms at the time of the CMD for the AR.

servations, we have assumed that the facular region has a rectangular shape whose fixed size is determined by the observations. We assume that the radiation for individual faculae, $I(\mu)_i$, is given by a relationship of the form of equation (3.1), with individual limb brightening coefficients a_i, b_i and c_i. The emission for individual faculae $I(\mu)_i$ is then integrated over the rectangle representing the active region; it is expected that this result should be similar to the angular distributions observed by VIRGO, as this instrument measures the radiation coming from the region as a whole. The coefficients for the individual faculae can be derived from integration of the data and therefore their emission. An example of the obtained results is shown in figure 3.11, where we present the observed CLV of the irradiance during CR 1911. Superposed are a fit to the observations, and the derived emission for individual faculae. Here we assume that every individual faculae radiates in the same manner. The rectangular source yields a wider angular distribution than that

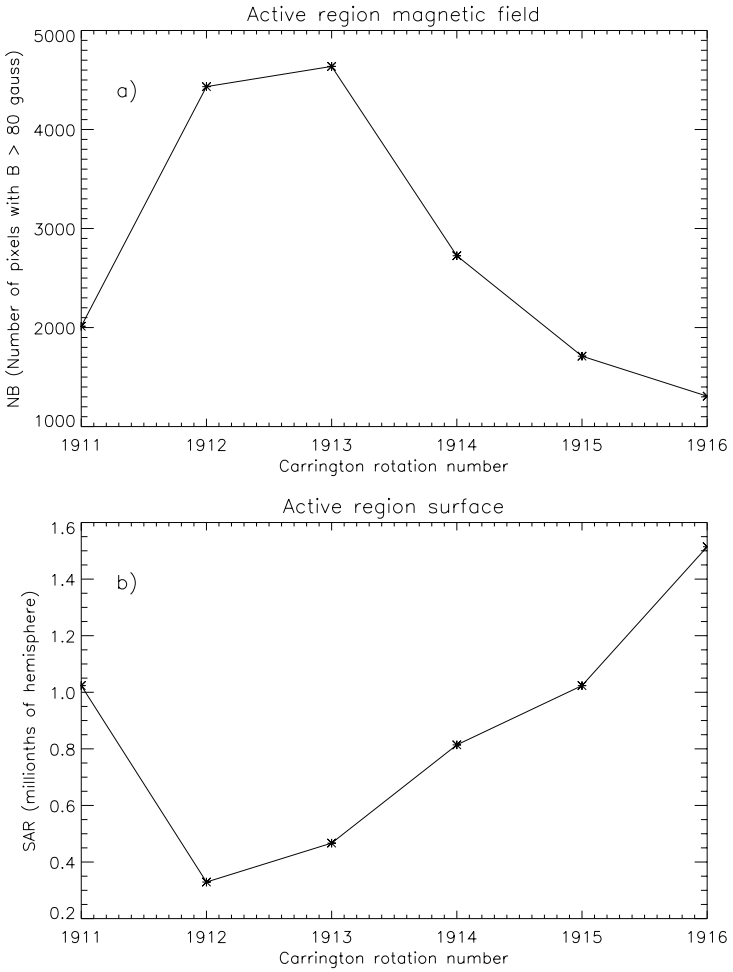

Figure 3.10: a) Evolution of the number of magnetic points (NB): number of pixels within the AR with B $>$ 80 gauss; b) Evolution of the active region surface (SAR): area that contains 90% of the points with B $>$ 80 gauss.

of the individual faculae. This result is consistent with what we can expect, as the region emits from all points considered therein. For clarity, both curves have been normalized at 45°. We are aware of the fact that assuming a rectangular shape for the facular region is a simplification which might lead to incorrect results.

Figure 3.12 shows the temporal and spectral evolution of the total facular emission, the volume under the 3-dimensional surface, for the three solar rotations dominated by faculae (CR's 1913, 1914 and 1915). The behaviour of the excess irradiance during CR's 1913 and 1914 is quite similar, while CR 1915 shows a decrease of the total facular emission probably due to the enlargement and spread out of the active region as it gets older. The wavelength dependence observed in this example is

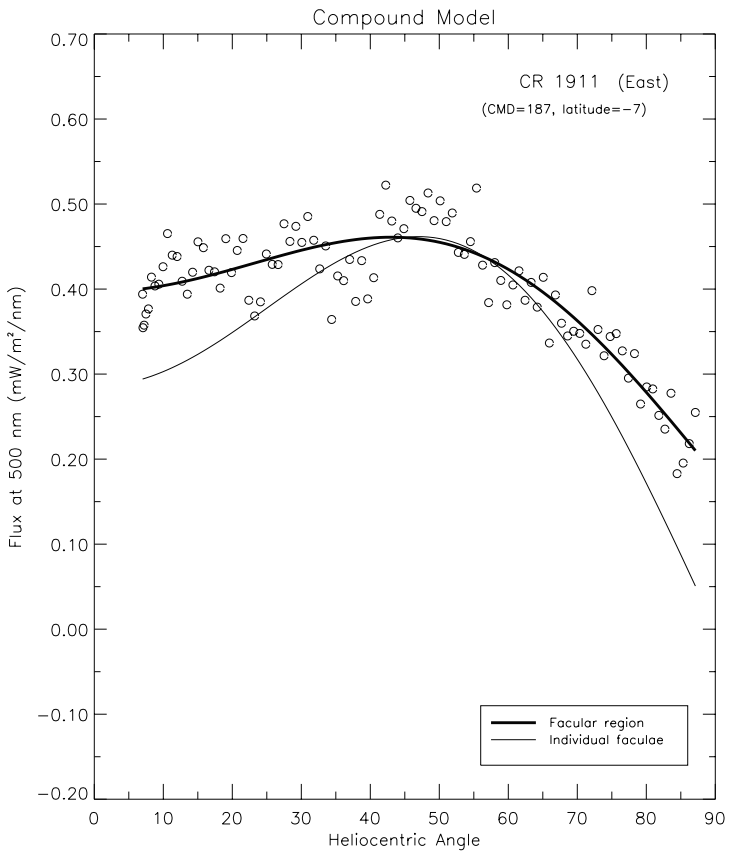

Figure 3.11: Observed angular distribution of the excess irradiance (circles) emitted by NOAA 7978 during CR 1911 (East of CMD) at 500 nm. The thick line is a fit to the observed CLV of the irradiance. It represents the whole facular region. The thin curve is the angular distribution of the irradiance emitted by an ideal single facula derived from the best fit to the data, in arbitrary units.

similar to the spectrum for faculae reported in earlier studies (Chapman & McGuire 1977; Lawrence 1987) and from theoretical models (Unruh et al. 1999). There is not a significant change in the wavelength dependence with the age of the active region.

3.5 Comparison with MDI

Equation (4.3) in Chapter 4 gives the intensity contrast, $C_{\rm fac}(\mu, B/\mu)$, for pixels with a given magnetic field strength, B/μ, and position over the solar disk, μ. These pixels are located simultaneously in MDI magnetograms and intensity im-

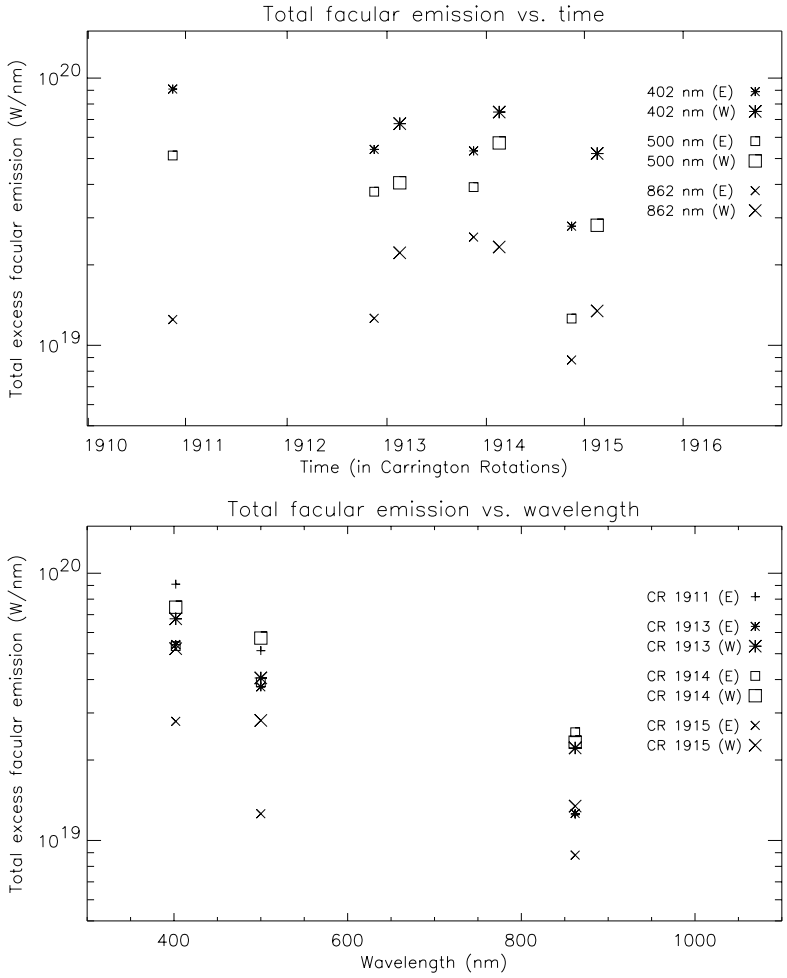

Figure 3.12: Top: Total spectral irradiance emitted by the active region versus time; bottom: Total spectral irradiance emitted by the active region versus wavelength. E and W mean, respectively, the East and the West disk passages of the AR.

ages (continuum at 676.8 nm). This expression was derived for the range of values $17\,\mathrm{G} \leq (B/\mu) \leq 600\,\mathrm{G}$ and $0.15 \leq \mu \leq 1$ (i.e., heliocentric angles between 0° and 80°). Nevertheless, care should be taken with data below $\mu = 0.4$ because of the unclear behaviour of the magnetic field projection at large heliocentric angles; for example, Hagenaar (2001) only considers pixels with $\theta < 60°$.

Using this equation we can predict the intensity for any given magnetic field within the range of validity of the equation. Since the relative intensity must be zero when the magnetic field becomes zero, it is reasonable to extrapolate equation (4.3) to the lowest magnetic field values. At the upper end of the magnetic field range, this 2-dimensional function appears to fit well high magnetic field values up to 600

G, although above 200 G some of the magnetic structures identified may be classified as micropores (since they are dark at small heliocentric angles). For each selected pixel in the magnetogram with coordinates (x, y), we "restore" the spectral intensity for a given value of B/μ by means of the expression:

$$I(x, y) = I(\mu) = C_{\rm fac}(\mu, |B/\mu|) LD(\mu) \tag{3.2}$$

where $C_{\rm fac}(\mu, B/\mu)$ is described in equation (4.3) and $LD(\mu)$ is the limb-darkening function used in Chapter 4. The relation between coordinates (x, y) and μ is given by $\sin\theta = \sqrt{x^2 + y^2}/R$ with R the solar radius in pixels. By integrating $I(x, y)$ over the entire solar disk we obtain the total spectral irradiance:

$$I_{\rm total}(B_1 \leq |B/\mu| \leq B_2) = \sum_{B_1, B_2} I(x, y) \tag{3.3}$$

where B_1 and B_2 are the limits of the B/μ range we are interested in. Finally, we normalize by the irradiance at 676.8 nm emitted by all pixels within the solar disk.

Figure 3.13 represents the total solar irradiance between 1 July 1996 and 31 December 1996, i.e., approximately the period when NOAA AR 7978 was present over the solar disk. This figure is based on data from the irradiance composite described in Fröhlich & Lean (1998a). Figure 3.14 shows the result of applying equation (3.3) to MDI magnetograms for the same period of time and for pixels with magnetogram signal $30\,{\rm G} \leq (B/\mu) \leq 180\,{\rm G}$. This range is intended to be an example representative of the smallest magnetic elements, and others values could have been chosen. This figure reproduces the relative spectral irradiance at 676.8 nm due to the network and faculae, without considering the sunspot influence. It should be noticed that we set the lower limit to 30 G because below this value, and even a bit above, the magnetograms show an undetermined amount of slowly varying noise somewhat time dependent.

When comparing figure 3.14 with figures 3.8 or 3.13, it is easily seen that there are significant differences between the restored values with respect to the observed total solar irradiance for each solar rotation. The reason is that the restored irradiance comes from magnetic field values that exclusively take into account the facular and network contributions, without sunspots, while the VIRGO measured total solar

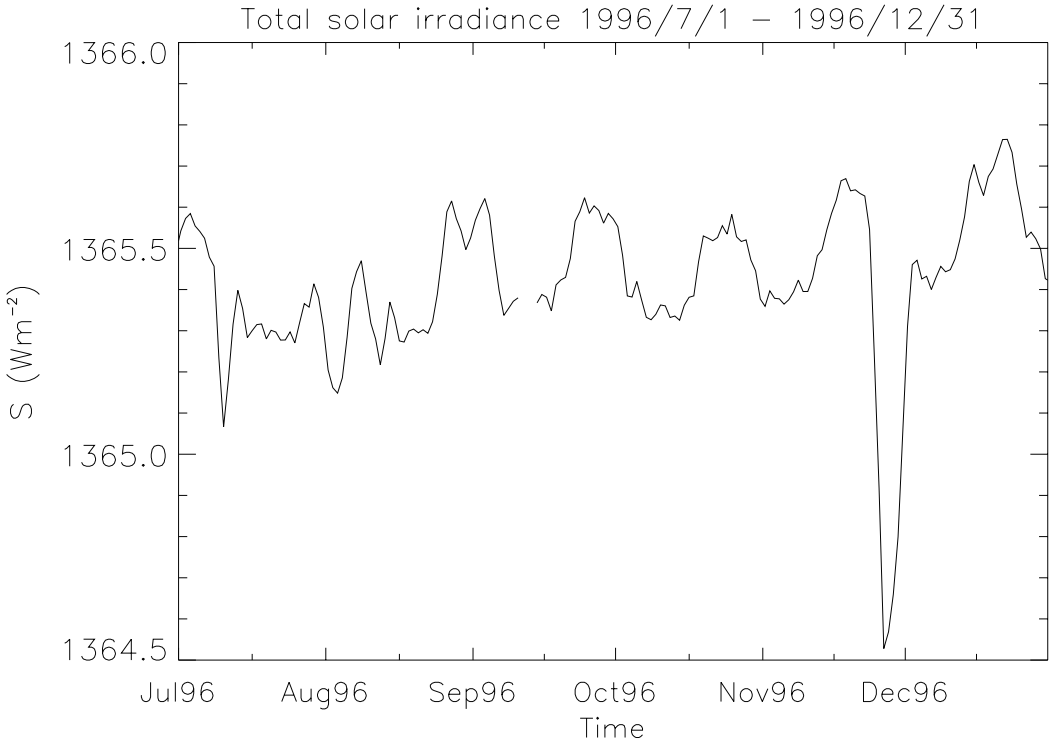

Figure 3.13: Total solar irradiance between 1 July and 31 December, 1996, as measured by the VIRGO radiometers. The period covers the passage of AR 7978 during seven CR's, from its birth in CR 1911 to its full dispersion during CR 1917. The PMOD/WRC (Switzerland) is acknowledged for providing the composite data.

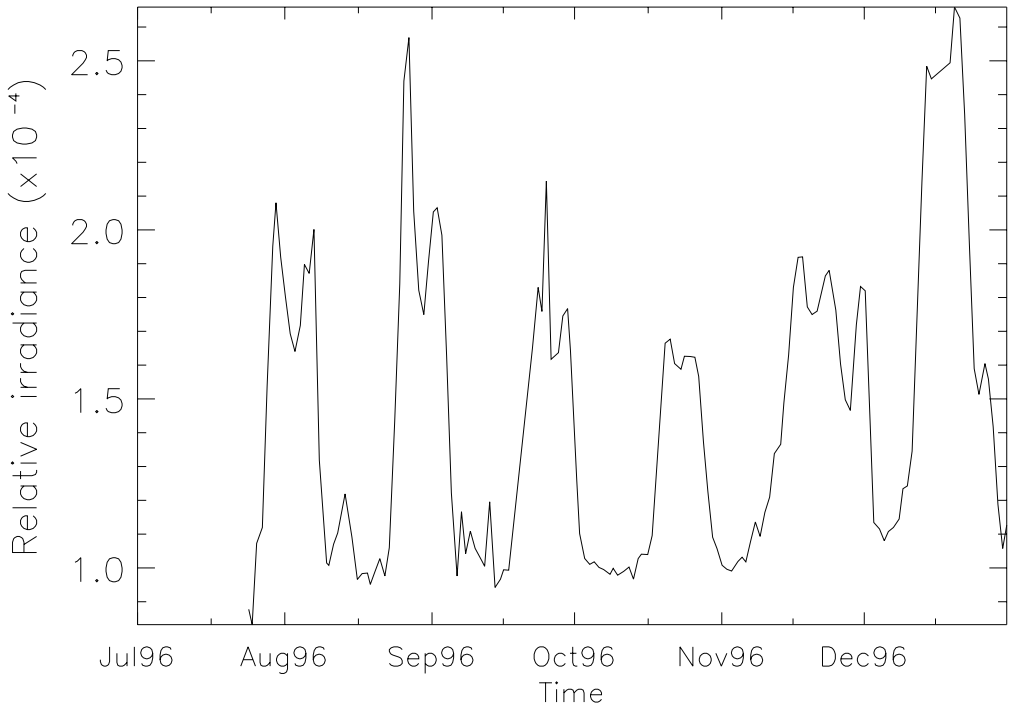

Figure 3.14: Relative spectral irradiance reconstruction for the same period of time choosing pixels with $30\,\mathrm{G} \leq (B/\mu) \leq 180\,\mathrm{G}$.

irradiance values also include the dark sunspots effects. In that sense, we point out that on CR 1912 there was a medium size sunspot (visible from 25 July to 8 August, 1996) that largely compensated the facular excess irradiance, and that on CR 1913 this sunspot become smaller although it was still contributing; during CR 1916 a few magnetic concentrations emerged, hosting a larger sunspot. The relative amplitude of the observed variations is also reproduced by the reconstruction, being approximately of $2\,10^{-4}$ relative to the mean value.

The reconstructed irradiance clearly shows the effect of the facular center-to-limb variation, particularly, note the double peaks during the active region passages. Evolution and peaks are sharper mainly because we have only used one magnetogram per day in the reconstruction, while VIRGO data is presented in hourly averages.

3.6 Discussion and Conclusions

A unique opportunity of observing a single AR on the solar disk has allowed us to study the global evolution of an active region with time. The fact that this AR had a relatively slow evolution allowed us to analyze it as if it was a permanent structure during every passage across the solar disk. We have analyzed the evolution of the global characteristics of the energy emission by the facular region associated with this AR, present during several solar rotations, at the minimum of solar activity. We studied the aging of NOAA AR 7978 using two parameters, the equivalent extent and the number of pixels with a line-of-sight photospheric magnetic field above a given magnetic threshold. The angular distribution of the excess radiance reflects the increase of the extension of the magnetic active region by becoming less limb-brightened as the region becomes older. By means of a simple phenomenological model we have derived the angular distribution for this facular region, as well as a tentative determination of the emission from individual facular elements.

By assuming a cylindrical symmetry for the facular region emission, we obtain the total (integrated in all directions) excess emission by the active region, as shown in figure 3.12. If we divide those values by the solar luminosity at the wavelengths of interest (taken from Thuillier et al. 1998), the global excess emission of the facular region appears to be of the order of $1.2\,10^{-4}$ of the solar luminosity at 402 nm during CR 1914, $0.8\,10^{-4}$ at 500 nm and $1.0\,10^{-4}$ at 862 nm. The wavelength dependence is similar to that reported in previous studies and does not change much with the

age of the region. The spectrum of the facular emission (figure 3.12, bottom panel) supports the theoretical spectrum derived by Unruh et al. (1999).

Finally, we have applied the function described in equation (4.3) to the case of the isolated active region NOAA AR 7978. This model predicts the contrast of photospheric bright features given a position on the disk and a magnetic signal value. From these contrasts we have reconstructed the relative spectral irradiance for the entire life of the studied AR. The result shows an excellent agreement between the reconstructed network and facular irradiances and the general profile of the total and spectral irradiance when there are no sunspots.